A Supplementary plots for LHCB-PAPER-2015-025

A.1 Comparison to previous experiments

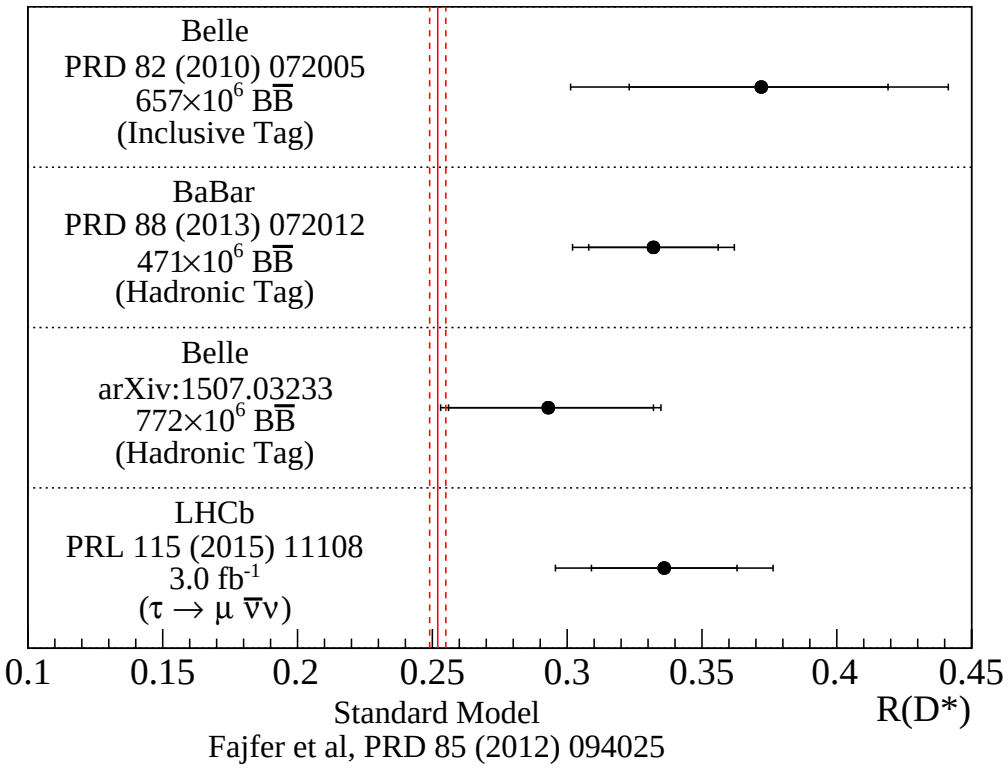

Figure 1: Comparison of the present result with recent B-factory measurements from Belle [1, 2] and BaBar [3, 4].

A.2 Detailed projections for control sample fits

Included here are the results of fits to the three background-enriched control samples shown in the same projections as Figure 1 in the paper.

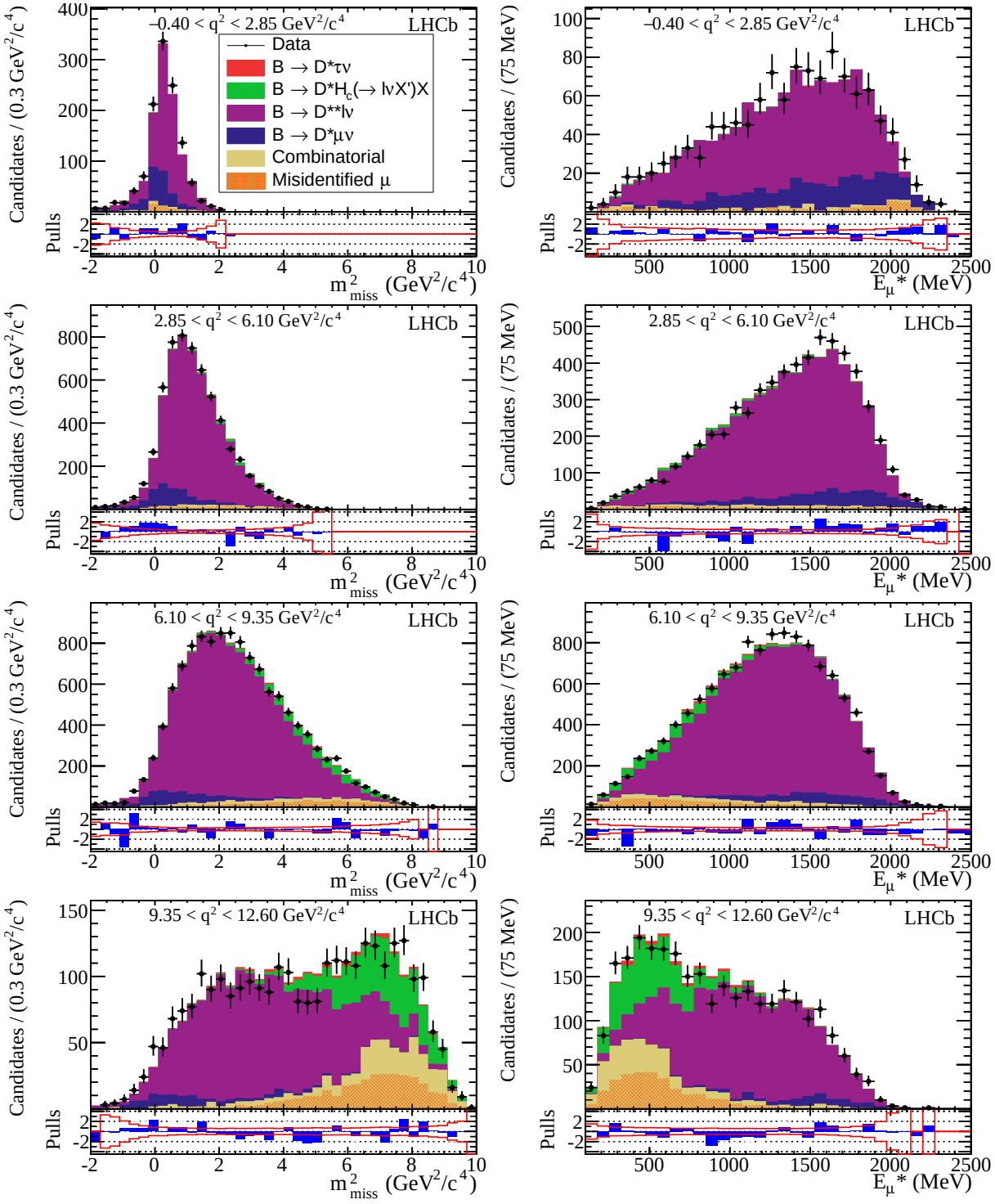

Figure 2: Results of fitting control data enriched in $\overline{B} \to [D_1, D_2^*, D_1']\mu^-\overline{\nu}_\mu$ (violet). The sample is selected requiring exactly one track selected by the isolation MVA with opposite charge to the D^{*+} candidate. Shown are projections in (left) $m^2_{\rm miss}$ and (right) E^*_μ for each bin of q^2.

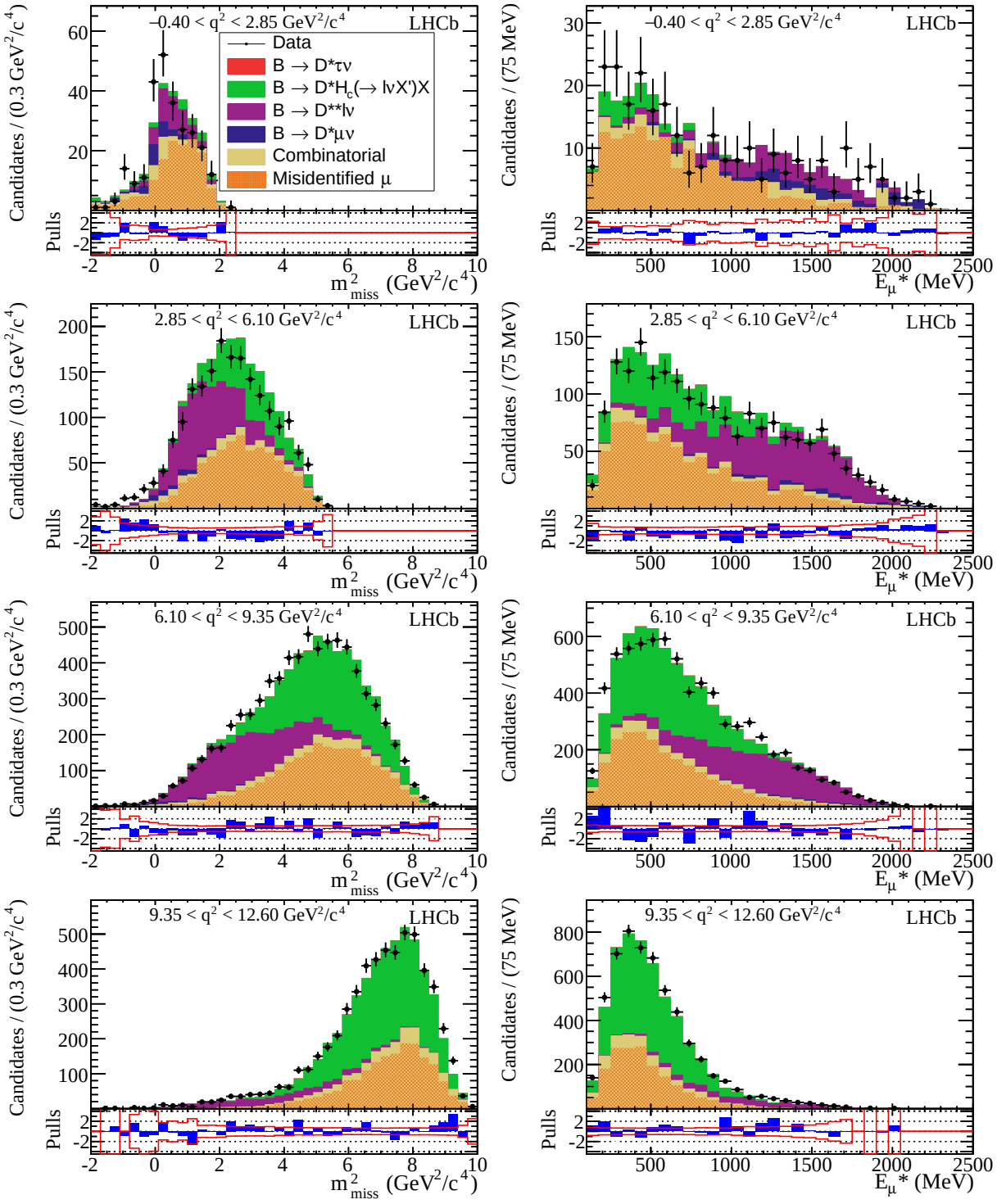

Figure 3: Results of fitting control data enriched in $\overline{B} \to D^{**}(\to D^{*+}\pi\pi)\mu^-\overline{\nu}_\mu$. The sample is selected requiring exactly two tracks with opposite charge selected by the isolation MVA. Shown are projections in (left) $m^2_{\rm miss}$ and (right) E^*_μ for each bin of q^2.

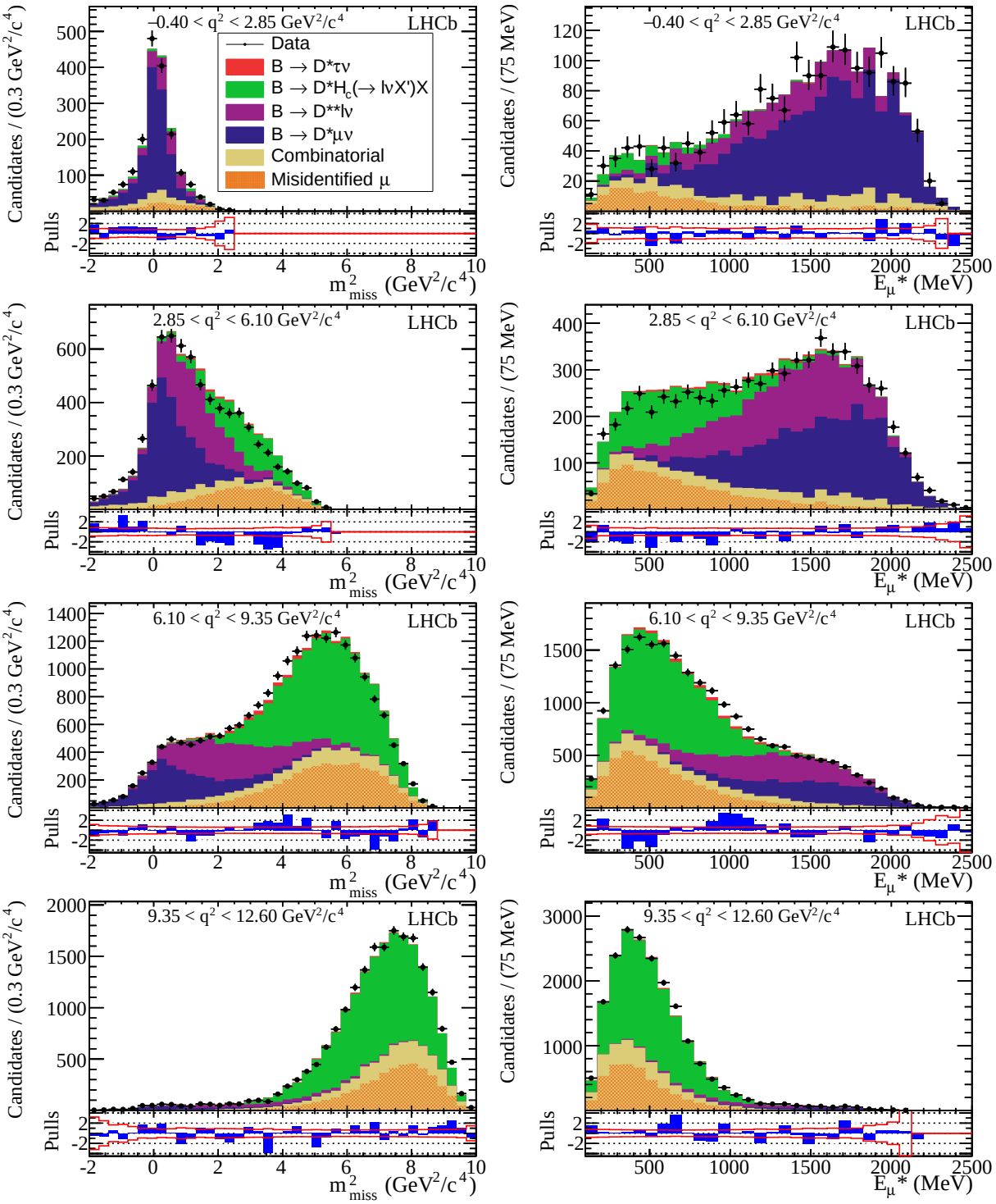

Figure 4: Results of fitting control data enriched in $B \to D^{*+}H_c(\to \mu\nu X')X$ (green). The sample is selected by requiring the isolation MVA identify a track consistent with originating from the B candidate vertex and at least one track consistent with the $K^{\pm}$ hypothesis near the B. Shown are projections in (left) $m^2_{\rm miss}$ and (right) E^*_μ for each bin of q^2.

A.3 Summed projections for all fits

Projections summed over q^2 bins.

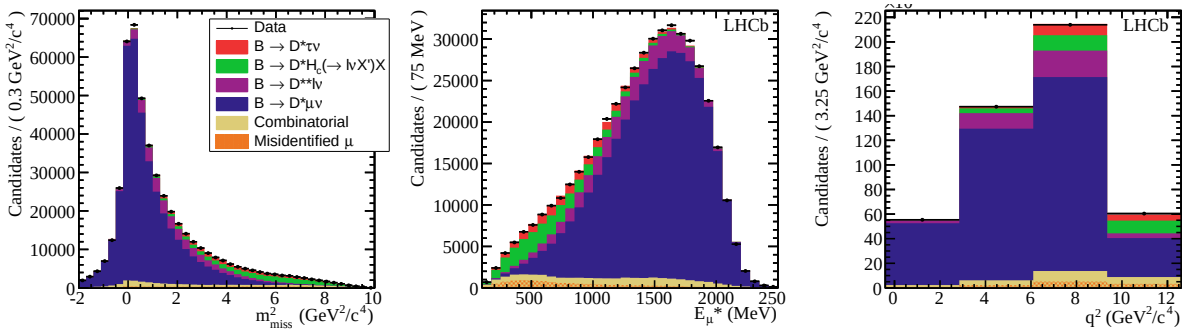

Figure 5: Distributions of (left) m^2_{miss} (center) E_μ and (right) q^2 for the signal sample with fit projections overlaid.

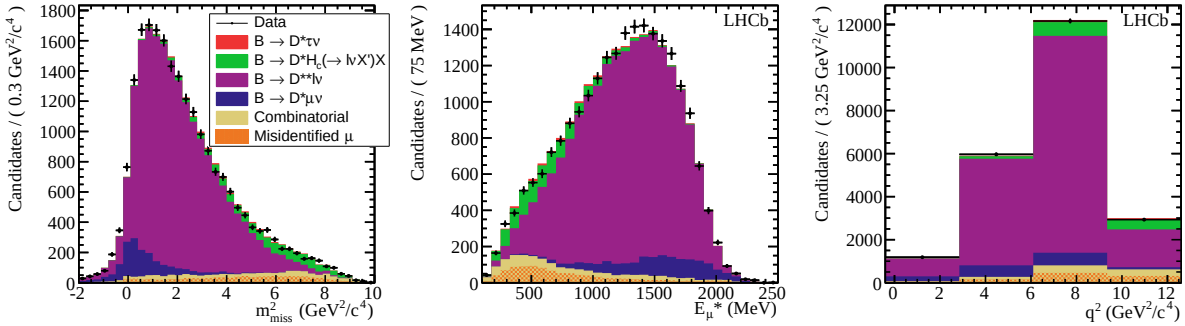

Figure 6: Distributions of (left) m^2_{miss} (center) E_μ and (right) q^2 for the $D^{*+}\mu^-\pi^-$ control sample with fit projections overlaid.

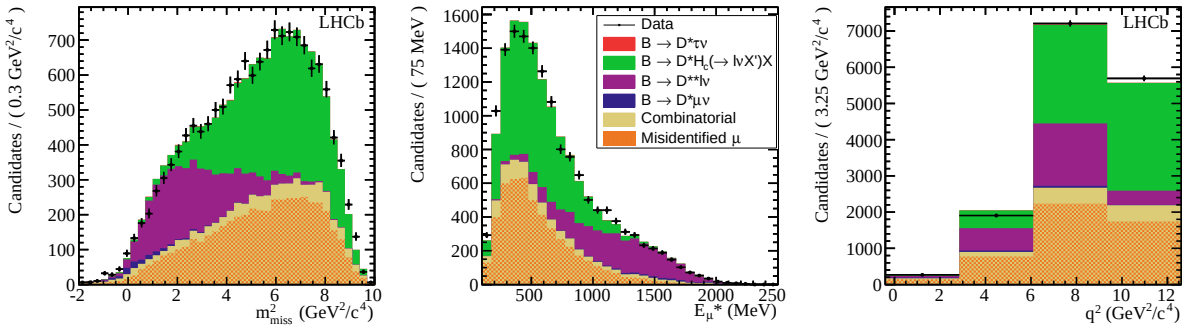

Figure 7: Distributions of (left) $m^2_{\rm miss}$ (center) E_μ and (right) q^2 for the $D^{*+}\mu^-\pi^+\pi^-$ control sample with fit projections overlaid.

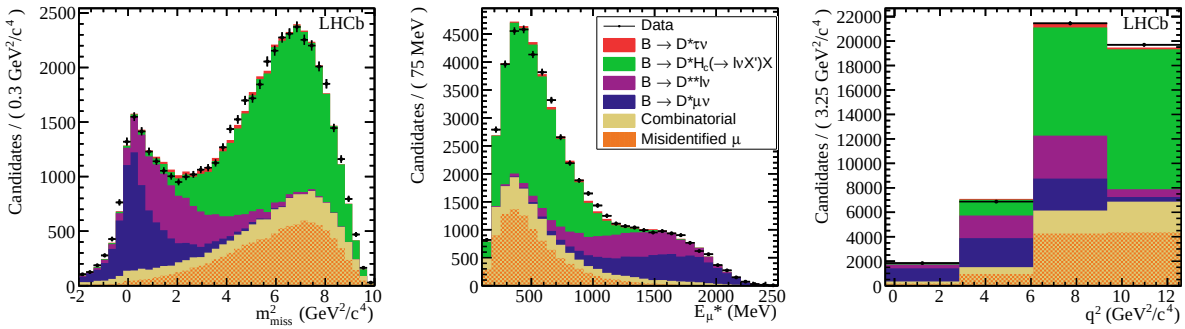

Figure 8: Distributions of (left) $m^2_{\rm miss}$ (center) E_μ and (right) q^2 for the $D^{*+}\mu^-K^\pm$ control sample with fit projections overlaid.

A.4 Template projections

Plots to illustrate rest-frame variables calculated for various illustrative backgrounds.

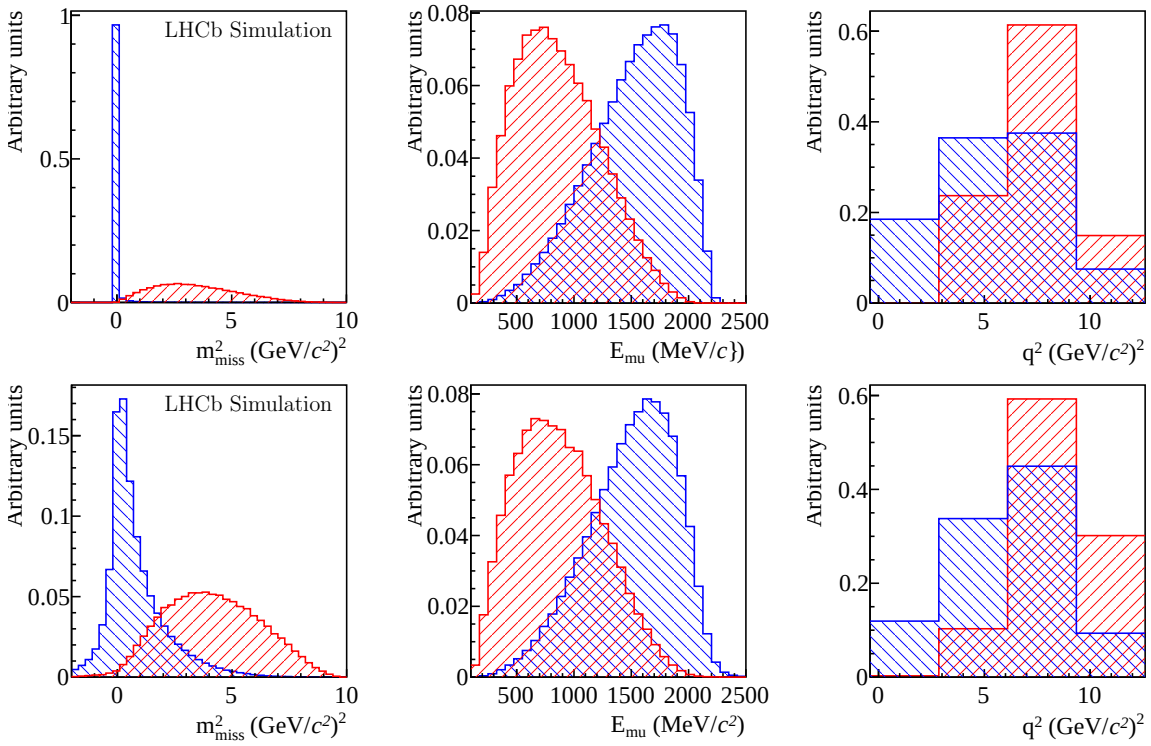

Figure 9: Distributions of (left) $m^2_{\rm miss}$ (middle) E^*_μ and (right) q^2 for simulated (blue) $\overline{B}^0 \to D^{*+}\mu^-\overline{\nu}_\mu$ and (red) $\overline{B}^0 \to D^{*+}\tau^-\overline{\nu}_\tau$ events events using (top) MC truth information and (bottom) reconstructed quantities.

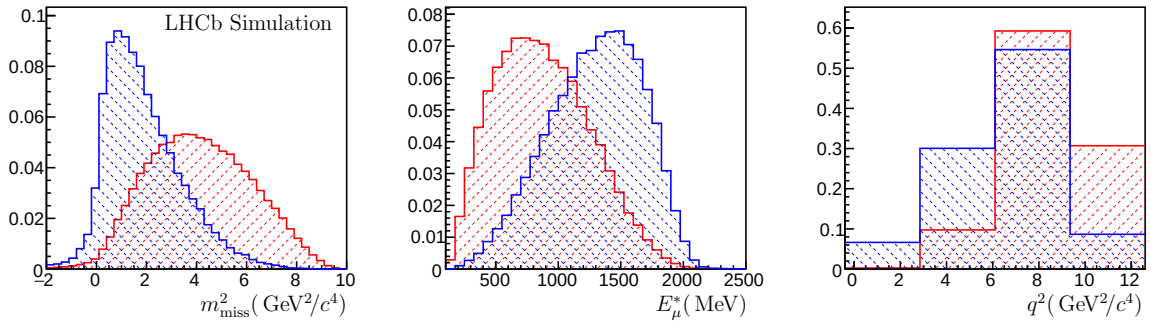

Figure 10: Distributions of (left) $m^2_{\rm miss}$ (middle) E^*_μ and (right) q^2 for simulated (blue) $B^0 \to D_1^+(2420)\mu^-\overline{\nu}_\mu$ and (red) $\overline{B}^0 \to D^{*+}\tau^-\overline{\nu}_\tau$ events.

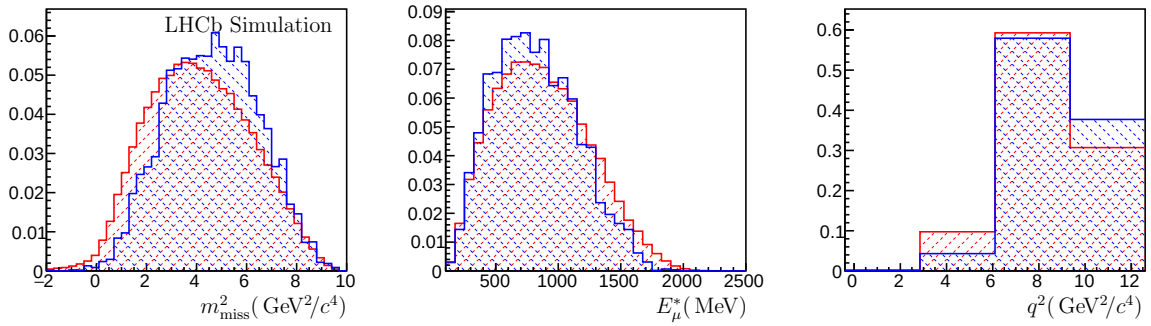

Figure 11: Distributions of (left) $m^2_{\rm miss}$ (middle) E^*_μ and (right) q^2 for simulated (blue) $\overline{B}^0 \to D_2^{*+}(2460)\tau^-\overline{\nu}_\tau$ and (red) $\overline{B}^0 \to D^{*+}\tau^-\overline{\nu}_\tau$ events.

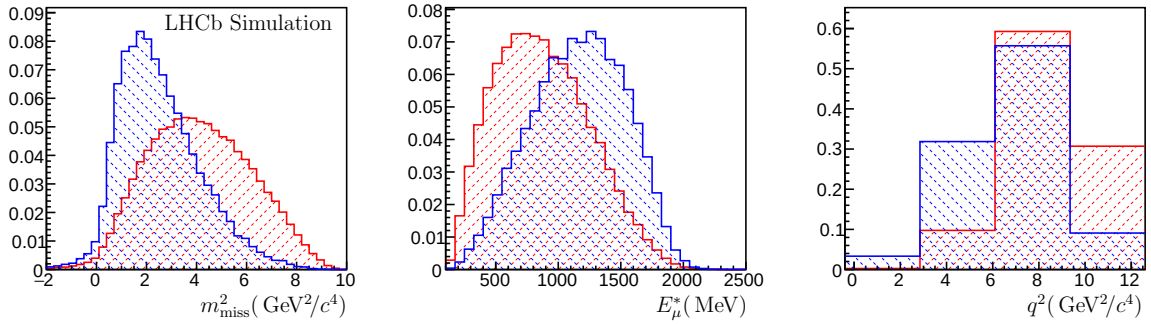

Figure 12: Distributions of (left) $m^2_{\rm miss}$ (middle) E^*_μ and (right) q^2 for simulated (blue) $\overline{B} \to D^{**}(\to D^{*+}\pi\pi)\mu^-\overline{\nu}_\mu$ and (red) $\overline{B}^0 \to D^{*+}\tau^-\overline{\nu}_\tau$ events.

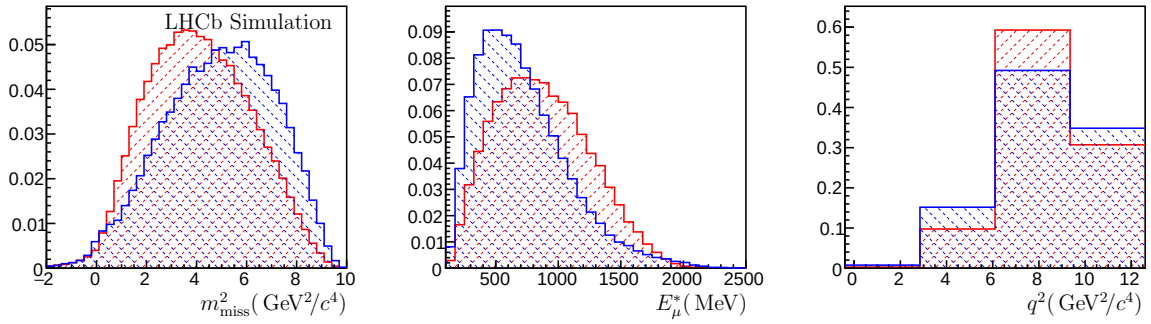

Figure 13: Projections in (left) $m^2_{\rm miss}$ (middle) E_μ and (right) q^2 for simulated (blue) $\overline{B}^0 \to D^{*+}H_c(\to \mu\nu X')X$ and (red) $\overline{B}^0 \to D^{*+}\tau^-\overline{\nu}_\tau$ events.

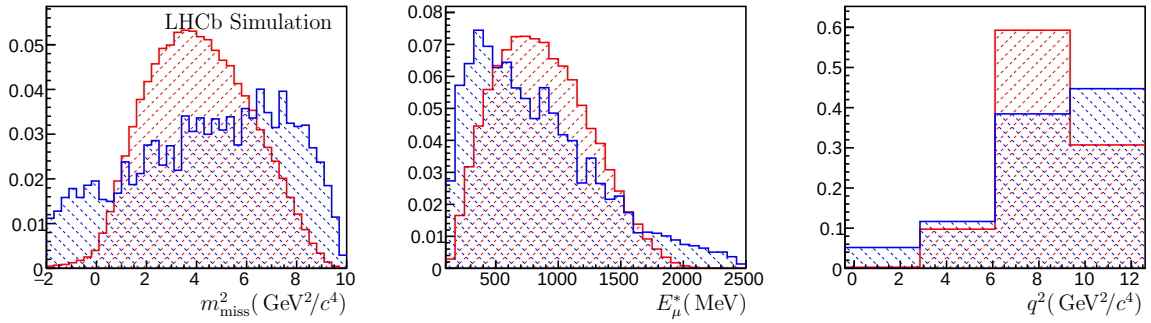

Figure 14: Projections in (left) $m^2_{\rm miss}$ (middle) E_μ and (right) q^2 for (blue) $D^{*+}\mu^+$ data (with hadron to muon misidentification and combinatorial D^* components removed) and (red) simulated $\overline{B}^0 \to\ D^{*+}\tau^-\overline{\nu}_\tau$ events.

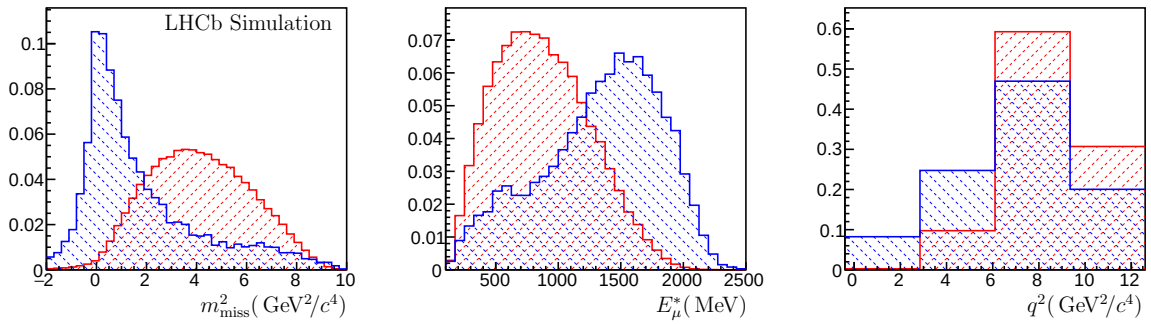

Figure 15: Projections in (left) $m^2_{\rm miss}$ (middle) E_μ and (right) q^2 for (blue) $D^0\pi^-\mu^+$ data and (red) simulated $\overline{B}^0 \to\ D^{*+}\tau^-\overline{\nu}_\tau$ events.

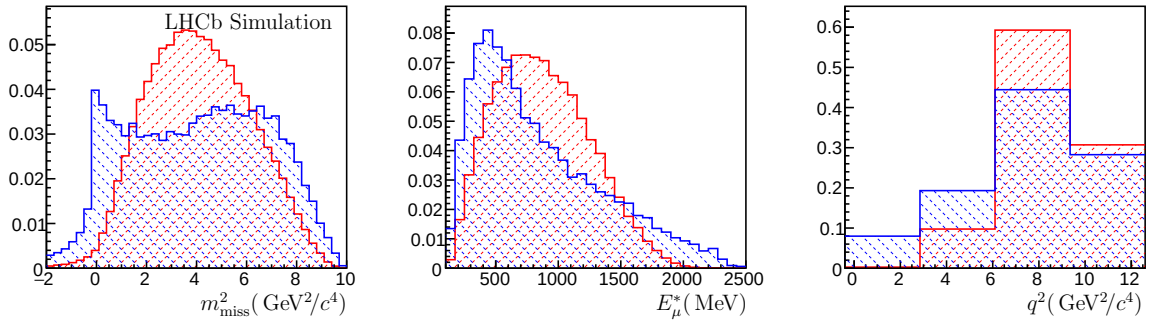

Figure 16: Projections in (left) $m^2_{\rm miss}$ (middle) E_μ and (right) q^2 for (blue) background from hadrons misidentified as muons and (red) simulated $\overline{B}^0 \to\ D^{*+}\tau^-\overline{\nu}_\tau$ events.

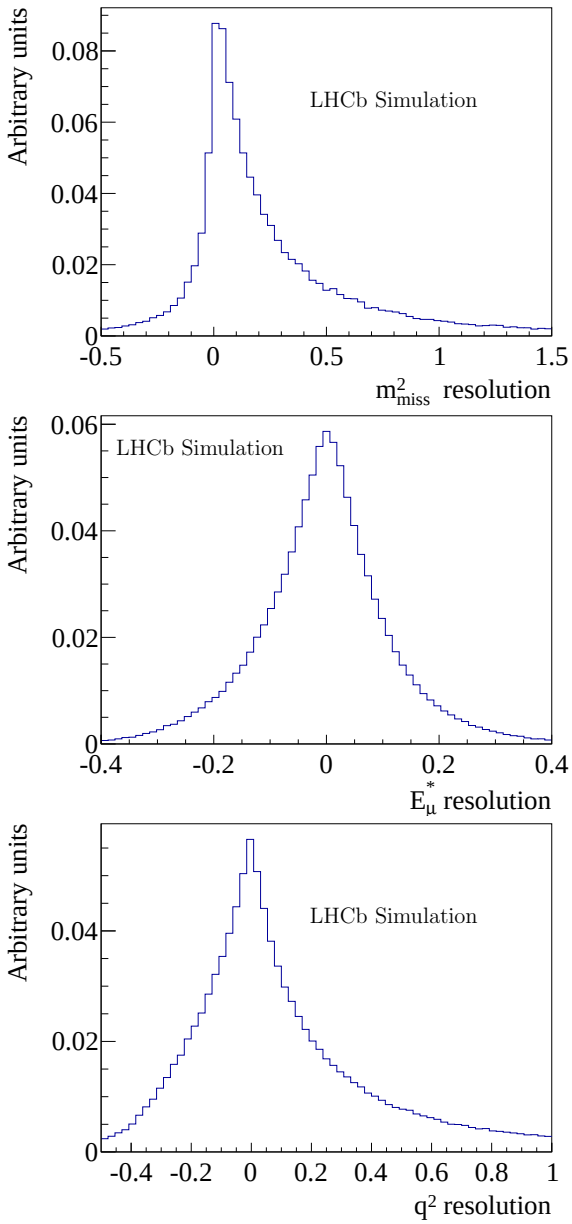

Figure 17: Resolution for (top) $m^2_{\rm miss}$ (middle) E_μ and (bottom) q^2 in simulated $B \to D^* \mu\nu$ events (defined as $\frac{\rm reco-true}{\rm true}$).

A.5 Isolation MVA output

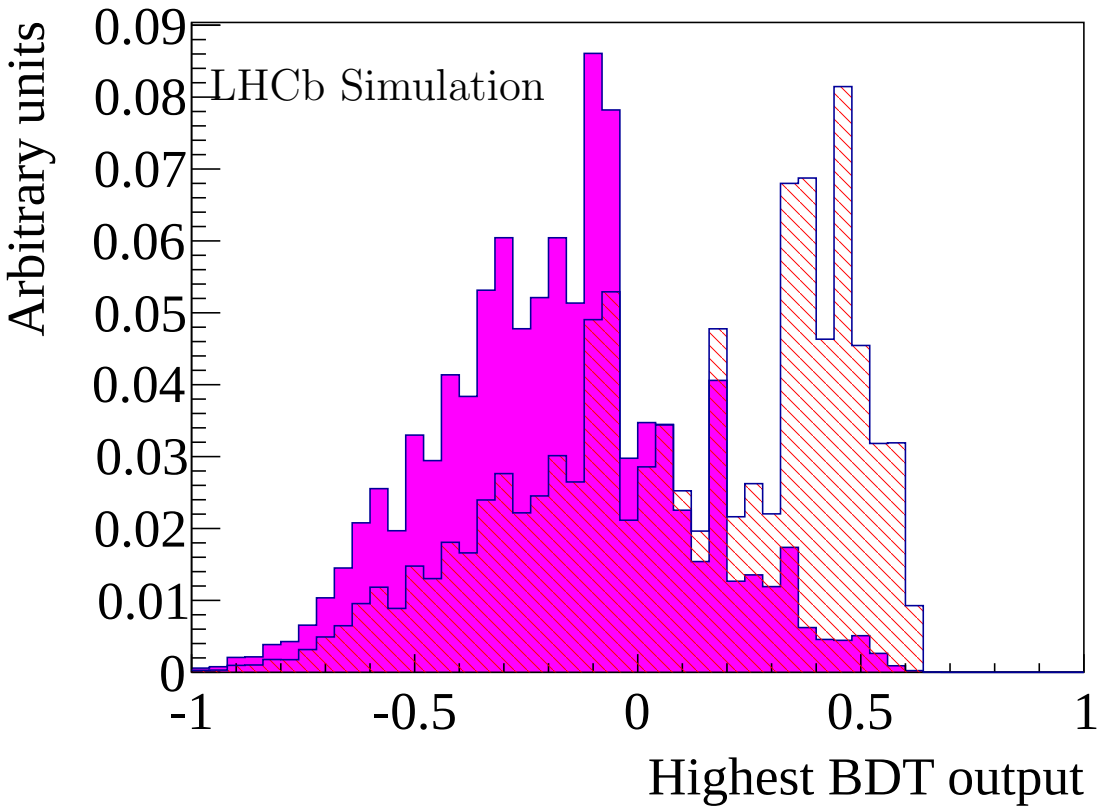

Figure 18: Distribution of largest isolation MVA output for any track in (solid) $B \to D^* \mu\nu$ and (hatched) $B \to D^{**} \mu\nu$ events.

References

[1] Belle collaboration, A. Bozek *et al.*, *Observation of $B^+ \to \overline{D}^{*0}\tau^+\nu_\tau$ and evidence for $B^+ \to \overline{D}^0\tau^+\nu_\tau$ at Belle*, Phys. Rev. **D82** (2010) 072005, arXiv:1005.2302.

[2] Belle collaboration, M. Huschle *et al.*, *Measurement of the branching ratio of $\bar{B} \to D^{(*)}\tau^-\bar{\nu}_\tau$ relative to $\bar{B} \to D^{(*)}\ell^-\bar{\nu}_\ell$ decays with hadronic tagging at Belle*, arXiv:1507.03233.

[3] BaBar collaboration, J. P. Lees *et al.*, *Evidence for an excess of $\bar{B} \to D^{(*)}\tau^-\bar{\nu}_\tau$ decays*, Phys. Rev. Lett. **109** (2012) 101802, arXiv:1205.5442.

[4] BaBar collaboration, J. P. Lees *et al.*, *Measurement of an excess of $\bar{B} \to D^{(*)}\tau^-\bar{\nu}_\tau$ decays and implications for charged Higgs bosons*, Phys. Rev. **D88** (2013) 072012, arXiv:1303.0571.